Electronic Supplementary Material (ESI) for Sustainable Energy & Fuels.

Supporting Information

Ultrathin Carbon-Coated Fe_7S_8 Core/Shell Nanosheets towards Superb Na Storage in both Ether and Ester Electrolyte Systems

Zhao Xiong, [a] Masayoshi Fuji [b,*] and Jisheng Zhou [a,*]

a. State Key Laboratory of Chemical Resource Engineering, Beijing Key Laboratory of Electrochemical Process and Technology for Materials, Beijing University of Chemical Technology, Beijing 100029, P. R. China.

b. Advanced Ceramics Research Center, Nagoya Institute of Technology, 3-101-1, Honmachi, Tajimi, Gifu 507-0033, Japan

* Corresponding authors: Tel/Fax: +86-10-64434916, zhoujs@mail.buct.edu.cn (J Zhou) fuji@nitech.ac.jp (M Fuji)

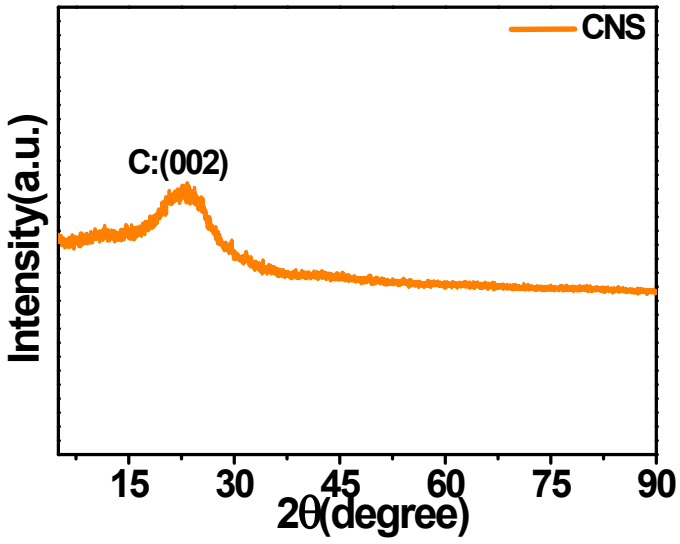

Figure S1. The XRD pattern of CNS shell obtained after removing Fe_7S_8 core in the Fe_7S_8@CNS composite.

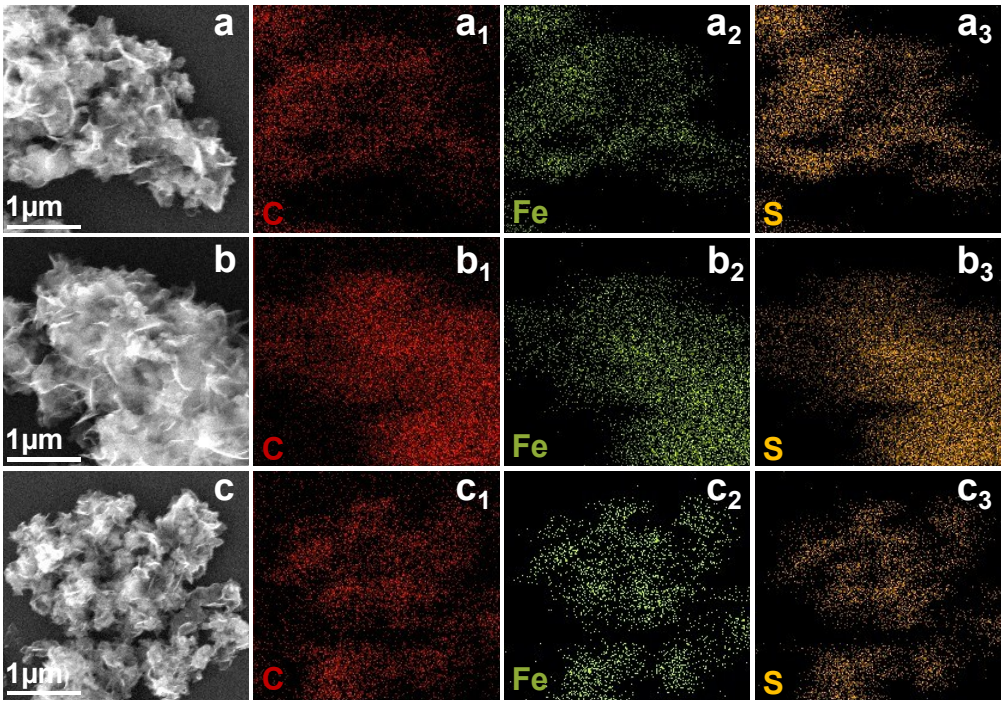

Figure S2. The elemental mapping images of (a) Fe_7S_8@CNS, (b) Fe_7S_8@CNS-600 and (c) Fe_7S_8@CNS-800.

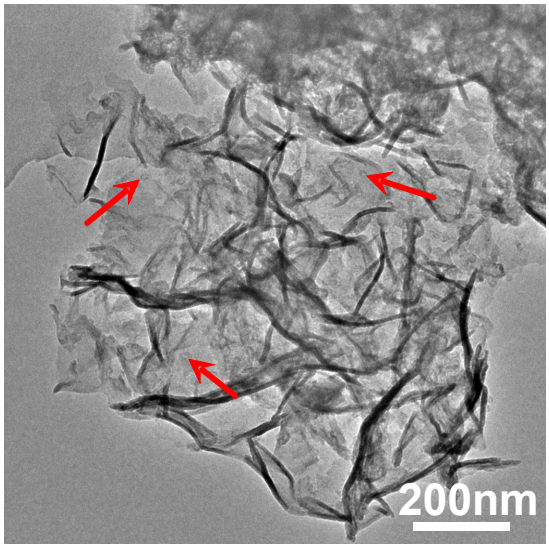

Figure S3. The TEM image of CNS shell obtained after removing Fe_7S_8 core in the Fe_7S_8@CNS composite.

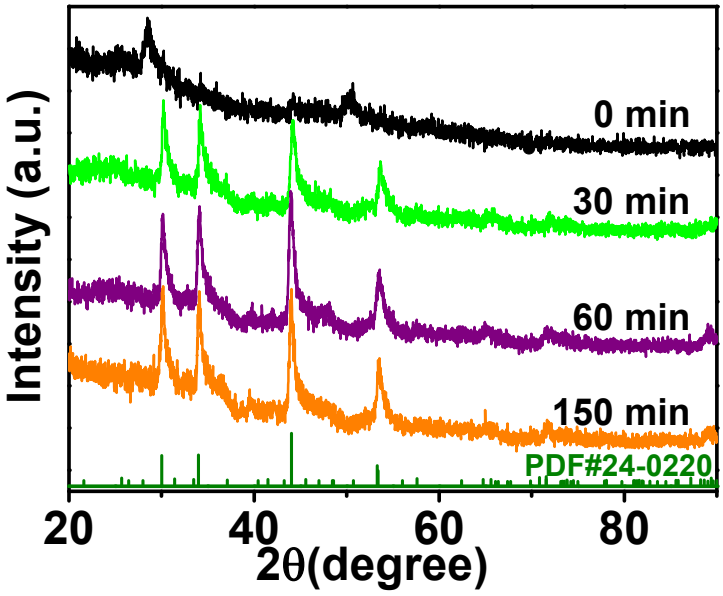

Figure S4. The XRD patterns of intermediates obtained at 500 °C with different holding time

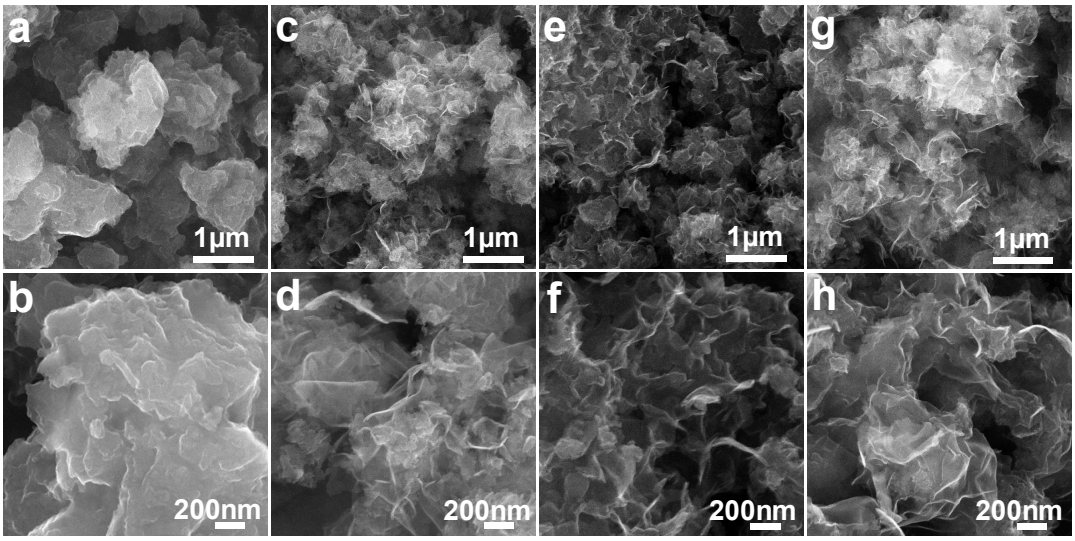

Figure S5. The SEM images of intermediates obtained at 500 °C with different holding time: (a, b) 0 min, (c, d) 30 min, (e, f) 60 min, and (g, h) 150 min.

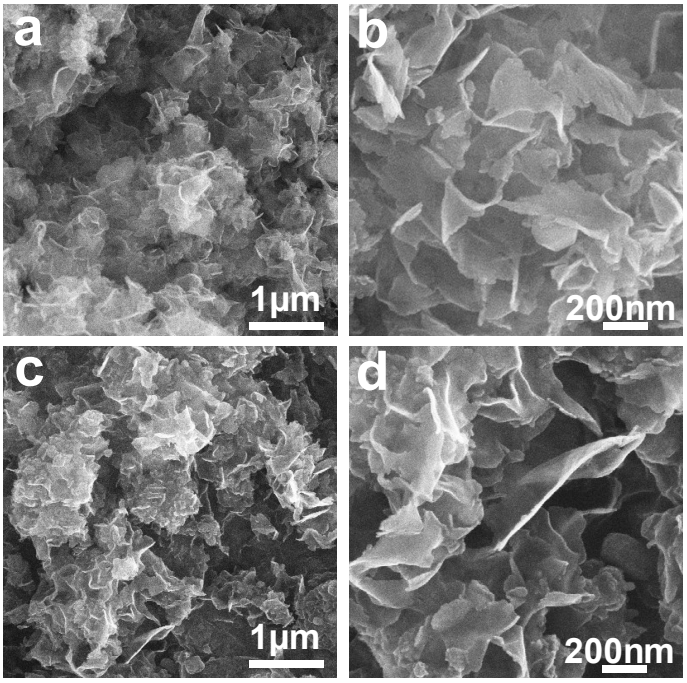

Figure S6. The SEM images of (a, b) Fe_7S_8@CNS-600 and (c, d) Fe_7S_8@CNS-800.

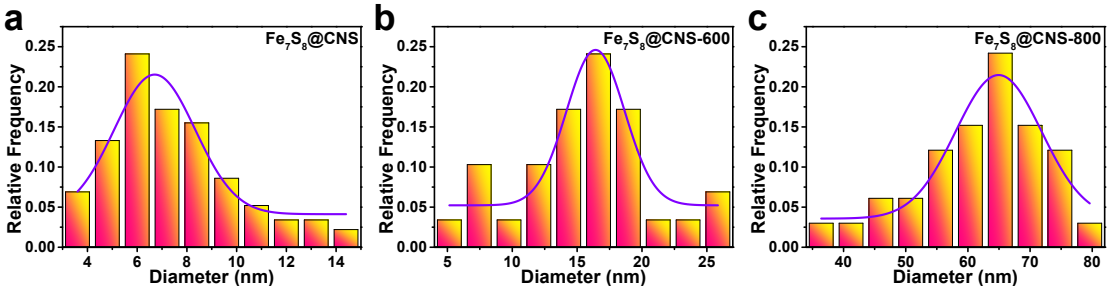

Figure S7. The diameter distribution of Fe_7S_8 nanosheets in (a) Fe_7S_8@CNS, (b) Fe_7S_8@CNS-600 and (c) Fe_7S_8@CNS-800.

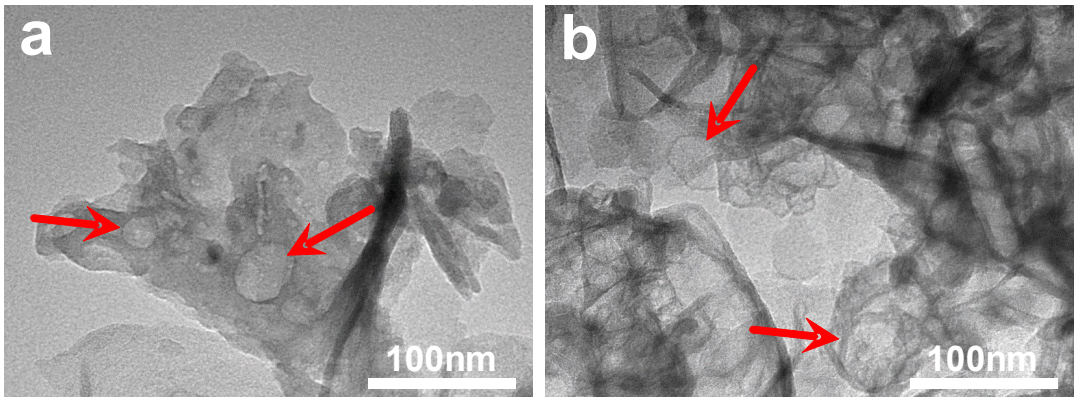

Figure S8. The TEM images of CNS shell obtained after removing Fe_7S_8 core in the (a) Fe_7S_8@CNS-600 and (b) Fe_7S_8@CNS-800.

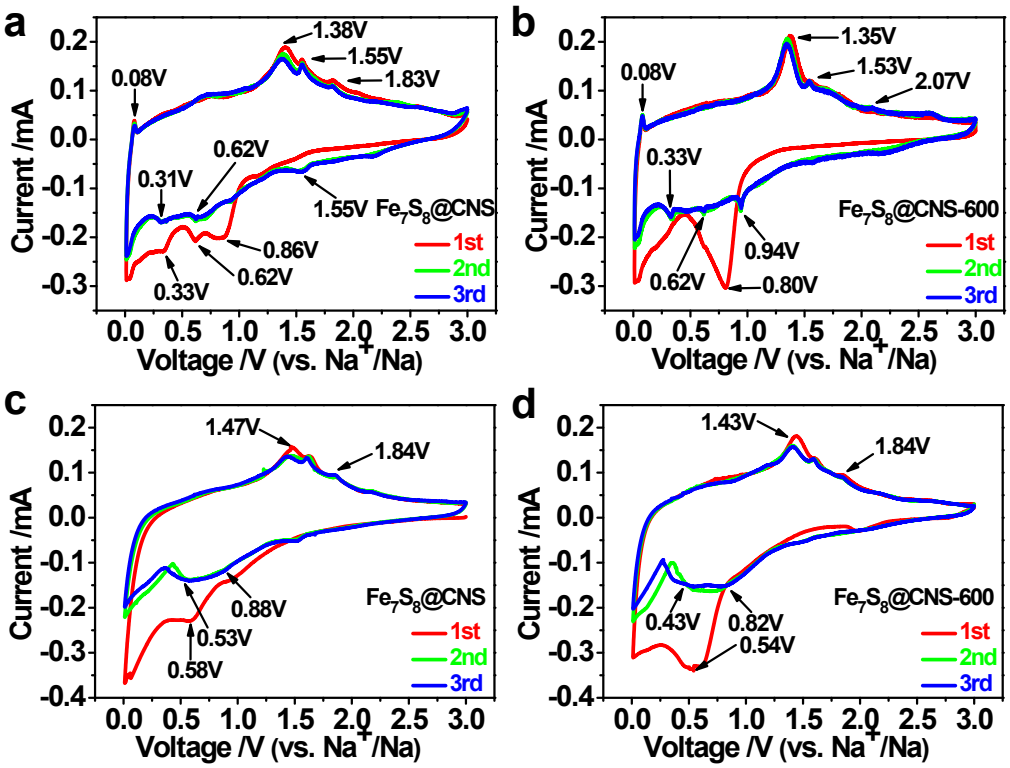

Figure S9. The CV curves of (a) Fe_7S_8@CNS and (b) Fe_7S_8@CNS-600 at the scan rate of 0.1 mVs^{-1} in a voltage window between 0.01 and 3 V with ether-based electrolyte, and (c) Fe_7S_8@CNS and (d) Fe_7S_8@CNS-600 at the scan rate of 0.1 mVs^{-1} in a voltage window between 0.01 and 3 V with ester-based electrolyte.

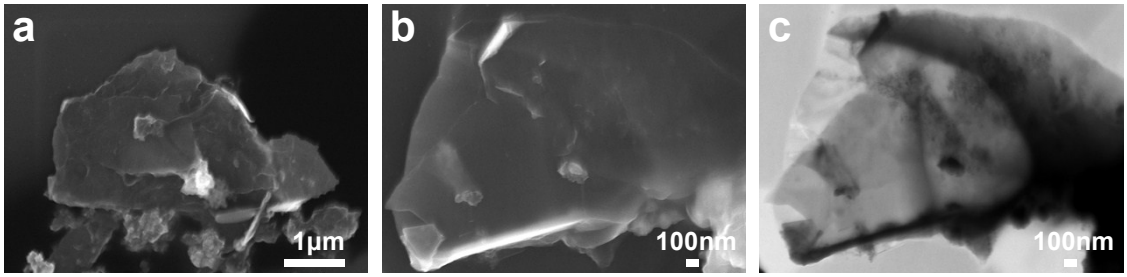

Figure S10. The SEM images (a, b) and TEM image (c) of Fe_7S_8@CNS-800 in the ether-based electrolyte after 4600 cycles at the current density of 10 A g^{-1}.

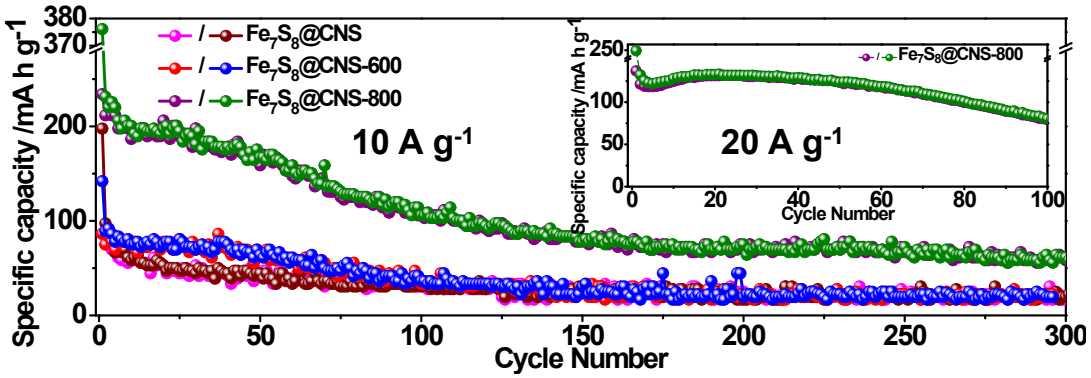

Figure S11. The cycling performance of Fe_7S_8@CNS, Fe_7S_8@CNS-600 and Fe_7S_8@CNS-800 in the ester-based electrolyte at 10 A g^{-1}; and the cycling performance (the inset) of Fe_7S_8@CNS-800 in the ester-based electrolyte at 20 A g^{-1}.

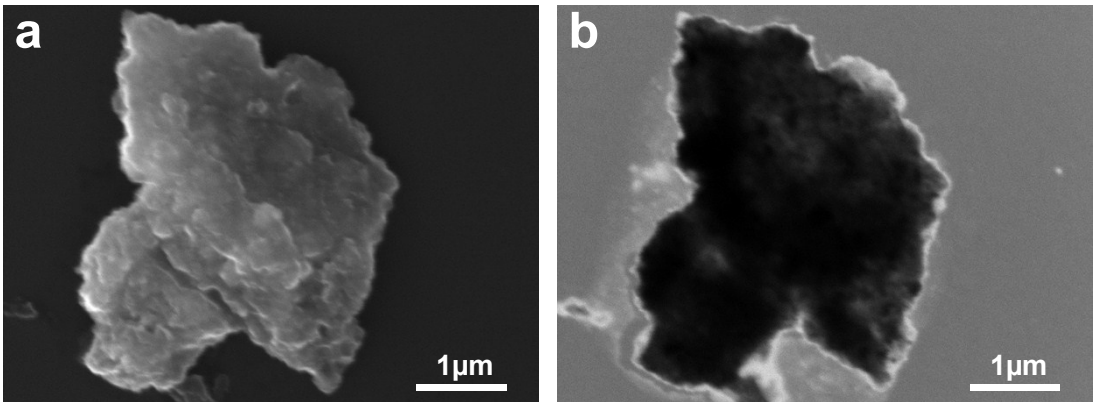

Figure S12. The SEM image (a) and TEM image (b) of Fe_7S_8@CNS-800 in the ester-based electrolyte after 4600 cycles at the current density of 10 A g^{-1}.

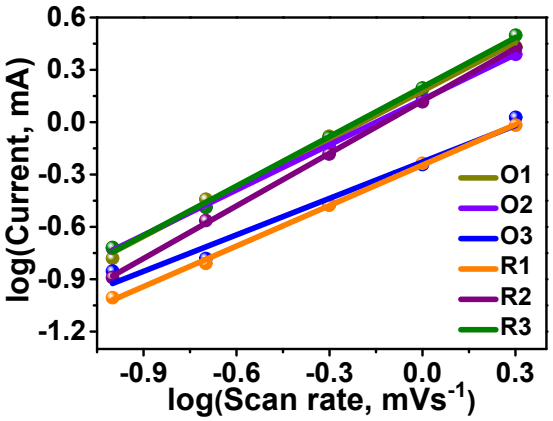

Figure S13. The linear plots (b) of peak current log (i) vs. scan rate log (v) of Fe_7S_8@CNS-800 in the ether-based electrolyte after 10 cycles at 0.1 A g^{-1}.

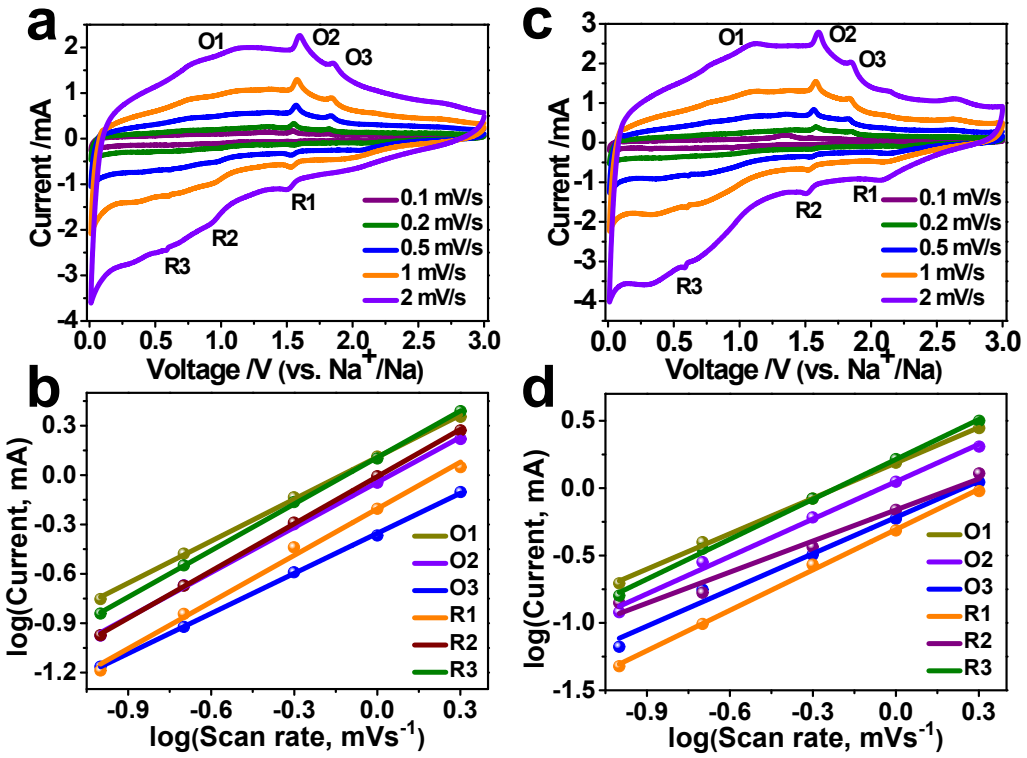

Figure S14. The CV curves at different scan rates for (a) Fe_7S_8@CNS and (c) Fe_7S_8@CNS-600 in the ether-based electrolyte after 10 cycles at 0.1 A g^{-1}; and corresponding linear plots of peak current log (i) vs. scan rate log (v) for (b) Fe_7S_8@CNS and (d) Fe_7S_8@CNS-600.

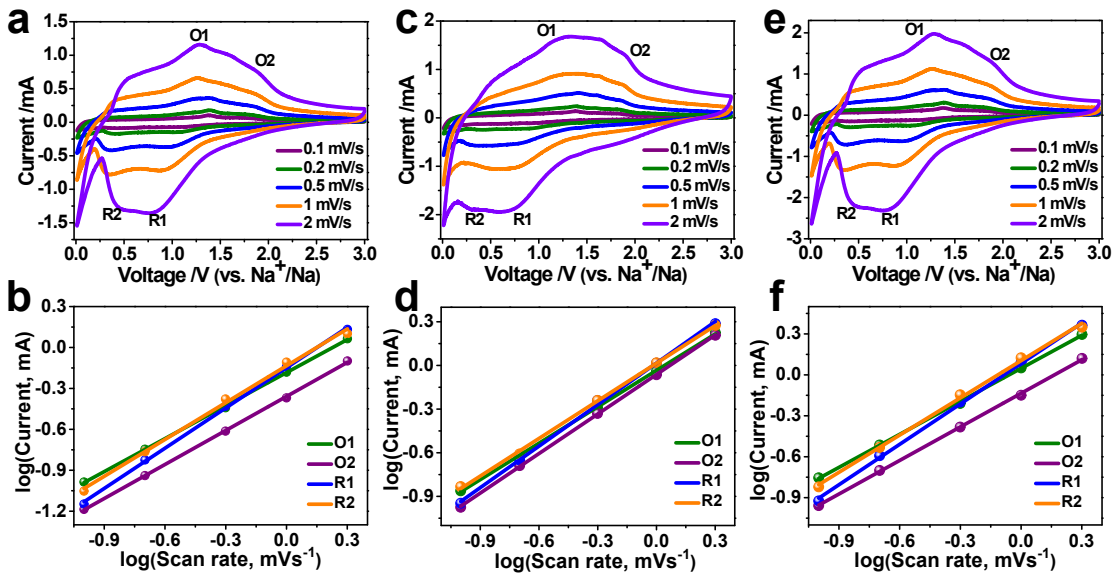

Figure S15. The CV curves at different scan rates for (a) Fe_7S_8@CNS, (c) Fe_7S_8@CNS-600 and (e) Fe_7S_8@CNS-800 in the ester-based electrolyte after 10 cycles at 0.1 A g^{-1}; and corresponding linear plots of peak current log (i) vs. scan rate log (v) for (b) Fe_7S_8@CNS, (d) Fe_7S_8@CNS-600 and (f) Fe_7S_8@CNS-800.

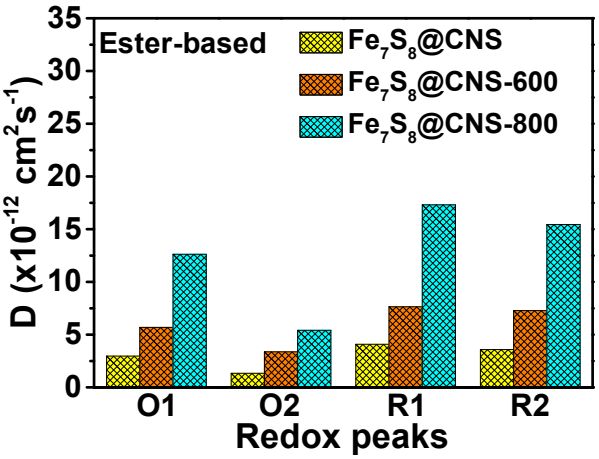

Figure S16. The histogram of diffusion coefficient for Fe_7S_8@CNS, Fe_7S_8@CNS-600 and Fe_7S_8@CNS-800 in the ester-based electrolyte.

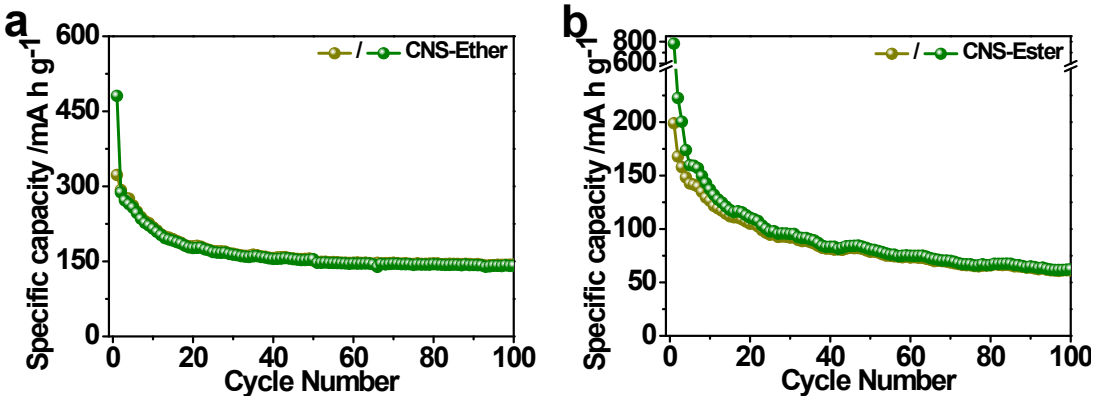

Figure S17. The cycling performances of CNS shell obtained after removing Fe_7S_8 core in the Fe_7S_8@CNS-800 in the (a) ether-based electrolyte and the (b) ester-based electrolyte at a current density of 100 mA g^{-1}.

Table S1. Electrochemical performance comparison for FeS_x as anode materials of SIBs in the ether-based electrolyte.

materials	Voltage range (V)	Current density	Initial reversible capacity	Initial coulombic efficiency	Rate performance	Cycle performance	Ref
FeS_2 nanoparticles	0.001-3.0	100 mA g^{-1}	490 mA h g^{-1}	64%	400 mA h g^{-1} at 100 mA g^{-1} 300 mA h g^{-1} at 500 mA g^{-1} 240 mA h g^{-1} at 1 A g^{-1}	300 mA h g^{-1} at 100 mA g^{-1} after 30 cycles	1
C/FeS microspheres	0.01-3.0	200 mA g^{-1}	661 mA h g^{-1}	80%	575 mA h g^{-1} at 100 mA g^{-1} 302 mA h g^{-1} at 1 A g^{-1} 164 mA h g^{-1} at 2 A g^{-1}	500 mA h g^{-1} at 200 mA g^{-1} after 45 cycles	2
FeS_2@C	0.1-2.0	100 mA g^{-1}	-	61.65%	525 mA h g^{-1} at 500 mA g^{-1} 502 mA h g^{-1} at 1 A g^{-1} 403 mA h g^{-1} at 5 A g^{-1}	511 mA h g^{-1} at 100 mA g^{-1} after 100 cycles	3
FeS_2/CNT	0.8-3.0	200 mA g^{-1}	534 mA h g^{-1}	74.6%	-	394 mA h g^{-1} at 200 mA g^{-1} after 400 cycles	4
FeS_2 particles	0.5-3.0	200 mA g^{-1}	524 mA h g^{-1}	72.7%	500 mA h g^{-1} at 200 mA g^{-1} 400 mA h g^{-1} at 2 A g^{-1} 323 mA h g^{-1} at 5 A g^{-1}	460 mA h g^{-1} at 200 mA g^{-1} after 800 cycles	5
FeS_2@$FeSe_2$	0.5-2.9	1 A g^{-1}	348.8 mA h g^{-1}	96.8%	486 mA h g^{-1} at 500 mA g^{-1} 456 mA h g^{-1} at 1 A g^{-1} 426 mA h g^{-1} at 2 A g^{-1}	350 mA h g^{-1} at 1 A g^{-1} after 2700 cycles	6
FeS_2/Co	0.8-2.9	1 A g^{-1}	-	90%	261 mA h g^{-1} at 1 A g^{-1} 192 mA h g^{-1} at 10 A g^{-1} 173 mA h g^{-1} at 20 A g^{-1}	220 mA h g^{-1} at 1 A g^{-1} after 5000 cycles	7
Fe_7S_8@C nanosheets	0.2-2.8	100 mA g^{-1}	540.7 mA h g^{-1}	90.6%	510.1 mA h g^{-1} at 100 mA g^{-1} 474 mA h g^{-1} at 200 mA g^{-1} 447.8 mA h g^{-1} at 500 mA g^{-1} 416.1 mA h g^{-1} at 1 A g^{-1} 386 mA h g^{-1} at 2 A g^{-1} 346.2 mA h g^{-1} at 5 A g^{-1} 243.1 mA h g^{-1} at 10 A g^{-1} 170.0 mA h g^{-1} at 20 A g^{-1}	310.2 mA h g^{-1} at 5 A g^{-1} after 2000 cycles and 243 mA h g^{-1} at 10 A g^{-1} after 4600 cycles and 170.0 mA h g^{-1} at 20 A g^{-1} after 8000 cycles	Our work

Table S2. Electrochemical performance comparison for FeS_x as anode materials of SIBs in the ester-based electrolyte.

materials	Voltage range (V)	Current density	Initial reversible capacity	Initial coulombic efficiency (%)	Rate performance	Cycle performance	Ref
FeS@C nanospheres	0.01-2.3	100 mA g^{-1}	722 mA h g^{-1}	70.2%	537 mA h g^{-1} at 500 mA g^{-1} 505 mA h g^{-1} at 1 A g^{-1} 452 mA h g^{-1} at 2.5 A g^{-1}	545 mA h g^{-1} at 100 mA g^{-1} after 100 cycles	8
FeS_x@C	0.01-2.5	100 mA g^{-1}	656.7 mA h g^{-1}	86%	577 mA h g^{-1} at 400 mA g^{-1} 514 mA h g^{-1} at 800 mA g^{-1} 403 mA h g^{-1} at 2 A g^{-1}	638.92 mA h g^{-1} at 100 mA g^{-1} after 100 cycles	9
FeS@grafitic carbon composite	0.01-2.4	50 mA g^{-1}	750 mA h g^{-1}	-	660 mA h g^{-1} at 50 mA g^{-1} 500 mA h g^{-1} at 500 mA g^{-1} 300 mA h g^{-1} at 4 A g^{-1}	742.9 mA h g^{-1} at 50 mA g^{-1} after 180 cycles	10
FeS/graphene composite	0.001-3.0	500 mA g^{-1}	530 mA h g^{-1}	71.6%	513 mA h g^{-1} at 1 A g^{-1} 424 mA h g^{-1} at 3 A g^{-1} 367 mA h g^{-1} at 5 A g^{-1}	547 mA h g^{-1} at 500 mA g^{-1} after 50 cycles	11
FeS@Fe3C@ graphitic carbon	0.01-2.3	100 mA g^{-1}	1015 mA h g^{-1}	60%	451 mA h g^{-1} at 1 A g^{-1} 347 mA h g^{-1} at 2 A g^{-1} 292 mA h g^{-1} at 5 A g^{-1}	575.7 mA h g^{-1} at 100 mA g^{-1} after 100 cycles	12
FeS@C/carbon cloth	0.5-3.0	0.15 C	500 mA h g^{-1}	64%	463 mA h g^{-1} at 0.15 C 390 mA h g^{-1} at 0.75 C 280 mA h g^{-1} at 7.5 C	430 mA h g^{-1} at 0.15 C after 50 cycles	13
FeS/carbon fibers	0.01-3.0	1 A g^{-1}	317 mA h g^{-1}	68.9%	438 mA h g^{-1} at 100 mA g^{-1} 332 mA h g^{-1} at 500 mA g^{-1} 247 mA h g^{-1} at 5 A g^{-1}	283 mA h g^{-1} at 1 A g^{-1} after 400 cycles	14
Fe_7S_8@C	0.01-3.0	100 mA g^{-1}	716.3 mA h g^{-1}	94.3%	661.9 mA h g^{-1} at 100 mA g^{-1} 591.7 mA h g^{-1} at 500 mA g^{-1} 537.2 mA h g^{-1} at 5 A g^{-1}	666.8 mA h g^{-1} at 100 mA g^{-1} after 100 cycles	15
FeS_2 nanocrystals	0.02-2.5	1 A g^{-1}	820 mA h g^{-1}	-	-	410 mA h g^{-1} at 1 A g^{-1} after 600 cycles	16
Fe_7S_8@C nanosheets	0.2-2.8	100 mA g^{-1}	398.6 mA h g^{-1}	65.8%	355.2 mA h g^{-1} at 100 mA g^{-1} 357.9 mA h g^{-1} at 200 mA g^{-1} 351.2 mA h g^{-1} at 500 mA g^{-1} 335 mA h g^{-1} at 1 A g^{-1} 306.5 mA h g^{-1} at 2 A g^{-1} 272 mA h g^{-1} at 5 A g^{-1} 105.9 mA h g^{-1} at 10 A g^{-1} 80.3 mA h g^{-1} at 20 A g^{-1}	156 mA h g^{-1} at 5 A g^{-1} after 2000 cycles and 61.3 mA h g^{-1} at 10 A g^{-1} after 300 cycles and 80.3 mA h g^{-1} at 20 A g^{-1} after 100 cycles	Our work

Table S3. b values at different redox potential peaks of Fe_7S_8@CNS, Fe_7S_8@CNS-600 and Fe_7S_8@CNS-800 in the ether-based electrolyte.

Ether	peak	O1	O2	O3	R1	R2	R3
Fe_7S_8@CNS	b-value	0.85	0.91	0.81	0.94	0.95	0.94
Fe_7S_8@CNS-600	b-value	0.88	0.93	0.89	0.99	0.76	0.98
Fe_7S_8@CNS-800	b-value	0.93	0.86	0.70	0.77	1.00	0.94

Table S4. b values at different redox potential peaks of Fe_7S_8@CNS, Fe_7S_8@CNS-600 and Fe_7S_8@CNS-800 in the ester-based electrolyte.

Ester	peak	O1	O2	R1	R2
Fe_7S_8@CNS	b-value	0.81	0.83	0.98	0.90
Fe_7S_8@CNS-600	b-value	0.83	0.91	0.95	0.86
Fe_7S_8@CNS-800	b-value	0.81	0.82	0.98	0.90

Table S5. The chemical diffusion coefficients of Fe_7S_8@CNS, Fe_7S_8@CNS-600 and Fe_7S_8@CNS-800 in the ether-based and ester-based electrolytes.

$D_{CV}(cm^2s^{-1})$	Ether	Ester
Fe_7S_8@CNS	$8.34x10^{-12}$	$2.99x10^{-12}$
Fe_7S_8@CNS-600	$1.03x10^{-11}$	$5.99x10^{-12}$
Fe_7S_8@CNS-800	$1.75x10^{-11}$	$1.26x10^{-11}$

Table S6. The fitting results of the EIS curves for the Fe_7S_8@CNS, Fe_7S_8@CNS-600 and Fe_7S_8@CNS-800 in the ether-based electrolyte.

Samples	Re (Ω)	Rf (Ω)	Rct (Ω)
Fe_7S_8@CNS	10.9	1.4	4.9
Fe_7S_8@CNS-600	10.1	3.6	3.1
Fe_7S_8@CNS-800	8.9	1.5	2.6

References

1. Z. Cao, H. Song, B. Cao, J. Ma, X. Chen, J. Zhou and Z. Ma, J. Power Sources, 2017, **364**, 208-214.
2. K. Zhang, M. Park, L. Zhou, G.-H. Lee, J. Shin, Z. Hu, S.-L. Chou, J. Chen and Y.-M. Kang, Angew. Chem. Int. Edit., 2016, **55**, 12822-12826.
3. Z. Liu, T. Lu, T. Song, X.-Y. Yu, X. W. Lou and U. Paik, Energy Environ. Sci., 2017, **10**, 1576-1580.
4. Y. Chen, X. Hu, B. Evanko, X. Sun, X. Li, T. Hou, S. Cai, C. Zheng, W. Hu and G. D. Stucky, Nano Energy, 2018, **46**, 117-127.
5. W. Zhao, C. Guo and C. M. Li, J. Mater. Chem. A, 2017, **5**, 19195-19202.

6. R. C. Anna Douglas, Landon Oakes, Keith Share, Adam P. Cohn, and Cary L. Pint, ACS Nano, 2015, **9**, 11156-11165.
7. K. Chen, W. Zhang, L. Xue, W. Chen, X. Xiang, M. Wan and Y. Huang, ACS Appl. Mater. Interfaces, 2017, **9**, 1536-1541.
8. Y. X. Wang, J. Yang, S. L. Chou, H. K. Liu, W. X. Zhang, D. Zhao and S. X. Dou, Nat. Commun., 2015, **6**, 8689.
9. Y. Tan, K. W. Wong, Z. Zhang and K. M. Ng, Nanoscale, 2017, **9**, 19408-19414.
10. H.-H. Fan, H.-H. Li, J.-Z. Guo, Y.-P. Zheng, K.-C. Huang, C.-Y. Fan, H.-Z. Sun, X.-F. Li, X.-L. Wu and J.-P. Zhang, J. Mater. Chem. A, 2018, **6**, 7997-8005.
11. S. Y. Lee and Y. C. Kang, Chem.-Eur. J., 2016, **22**, 2769-2774.
12. Q. Wang, W. Zhang, C. Guo, Y. Liu, C. Wang and Z. Guo, Adv. Funct. Mater., 2017, **27**, 1703390.
13. X. Wei, W. Li, J. A. Shi, L. Gu and Y. Yu, ACS Appl. Mater. Interfaces, 2015, **7**, 27804-27809.
14. D. Li, Y. Sun, S. Chen, J. Yao, Y. Zhang, Y. Xia and D. Yang, ACS Appl. Mater. Interfaces, 2018, **10**, 17175-17182.
15. L. Shi, D. Li, J. Yu, H. Liu, Y. Zhao, H. Xin, Y. Lin, C. Lin, C. Li and C. Zhu, J. Mater. Chem. A, 2018, **6**, 7967-7976.
16. M. Walter, T. Zund and M. V. Kovalenko, Nanoscale, 2015, **7**, 9158-9163.